PM Axial Flux Machine Design for Hybrid Traction

Olivier de La Barrière, S. Hlioui, H. Ben Ahmed, Mohamed Gabsi, M. Lobue

Oil & Gas Science and Technology – Rev. IFP, Vol. 65 (2010), No. 1, pp. 203-218

DOI: 10.2516/ogst/2009058

IFP International Conference
Rencontres Scientifiques de l'IFP

Advances in Hybrid Powertrains
Évolution des motorisations hybrides

PM Axial Flux Machine Design for Hybrid Traction

O. de la Barrière, S. Hlioui, H. Ben Ahmed, M. Gabsi and M. LoBue

SATIE, ENS Cachan, CNRS, UniverSud, 61 avenue du Président Wilson, 94230 Cachan - France
e-mail: olivier.de-la-barriere@satie.ens-cachan.fr - hlioui@satie.ens-cachan.fr - hamid.benahmed@bretagne.ens-cachan.fr
gabsi@satie.ens-cachan.fr - martino.lo-bue@satie.ens-cachan.fr

Résumé — Conception d'une machine à flux axial à aimants permanents pour la traction hybride — La traction hybride semble actuellement un des moyens les plus prometteurs pour réduire la consommation de carburant des véhicules. Ce procédé consiste à associer un moteur électrique au moteur thermique traditionnel. Pour une telle application embarquée, le rendement, ainsi que le couple massique, sont des critères de conception de première importance. Dans ce contexte, le recours à une machine synchrone à aimants permanents, reconnue pour satisfaire ces deux critères, semble être approprié. Vu que le volume alloué à la machine électrique est de forme discoïde, les topologies à flux axial semblent les plus intéressantes. L'objectif de cet article est de proposer une méthodologie de pré-dimensionnement de tels actionneurs, en ayant fixé au préalable le volume maximal permis ainsi que le cahier des charges de la machine.

Abstract* — *PM Axial Flux Machine Design for Hybrid Traction — *Hybrid traction seems to be one of the best ways in order to reduce fuel consumption for vehicles. It consists of associating an electric motor next to the classical thermal machine. In this embedded system, the efficiency and the torque per unit mass are very important. So it seems to be a good idea to use a permanent magnet synchronous machine, which is recognized for satisfying these two objectives. Since the allocated volume is rather flat, axial flux topologies are interesting. This paper's goal is to propose an optimal first design method for such structures, given the allocated volume and the machine requirements.*

INTRODUCTION

For both economic and environmental reasons, it is becoming necessary to reduce fuel consumption of cars. The association of an electric motor to the thermal one, which is called hybrid traction, is one of the most interesting solutions for that. We are going to use an axial flux permanent magnet machine, for its flat shape. After the presentation of the machine, we would like to propose an optimization strategy for the design of the electric machine, based on the use of evolutionary algorithms. Then, we will describe briefly the model used for the optimization. To finish, a few optimization results will be presented, and analyzed.

1 PRESENTATION OF THE MACHINE

There are a lot of axial flux permanent magnet machines structures [1]. The basic one is composed of a rotor with alternated polarity permanent magnets, placed in front of a laminated stator carrying a multiphase winding. There are also multi-layers structures, but most of them can be seen as a composition of single-layers ones.

We are just going to study the single layer machine in this article. The detailed topology is drawn in Figure 1a. Water cooling is employed, so as to remove the loss in a more efficient way than simple air natural convection. As we will see, since flux weakening capabilities are required, we choose a rotor with salient poles *(Fig. 1b)*. The stator is also shown in Figure 1c, and the two parts together are represented in Figure 1d.

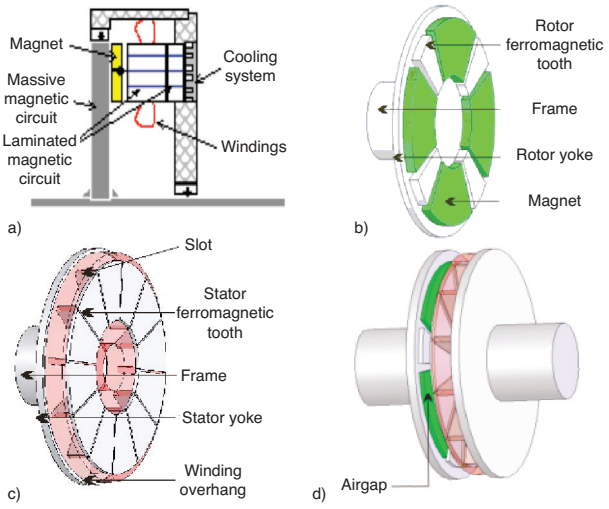

Figure 1

Presentation of the studied machine. a) Sectional representation of the machine. b) The salient rotor. c) The stator. d) The whole machine.

2 THE OPTIMIZATION STRATEGY

We are going to describe our optimization method. More precisely, given the application requirements, and data about the materials which will be used, the purpose consists on reversing the mathematical model in order to provide the best geometrical parameters for chosen optimization criteria.

2.1 Optimization Problem Presentation

Every optimization problem is clearly defined once the following points are given:

- a single or several objectives, which will have to be minimized;
- parameters, evolving on a permitted domain;
- restrictions to be observed so as to get allowable solutions.

These three points have to be detailed for our problem.

2.1.1 Optimization Objectives

Since the motor is designed for an embedded system, it seems to be important to minimize both its mass and its working losses, which are two contradictory criteria. So it is a multi-objectives optimization problem. Multi-objective optimization results are Pareto's curve, composed of all the closest point to the ideal point, which is the zero mass and zero losses point, and is of course impossible to reach. Each point on this curve represents a different, but optimal compromise between the two objectives.

The optimization of the hybrid system must be carried out for a cycle of points [3] in the torque *vs* speed plan that the electric machine must be able to reach *(Fig. 2)*.

The best thing to do is certainly to carry out the mass and losses minimization strategy for a working cycle of the

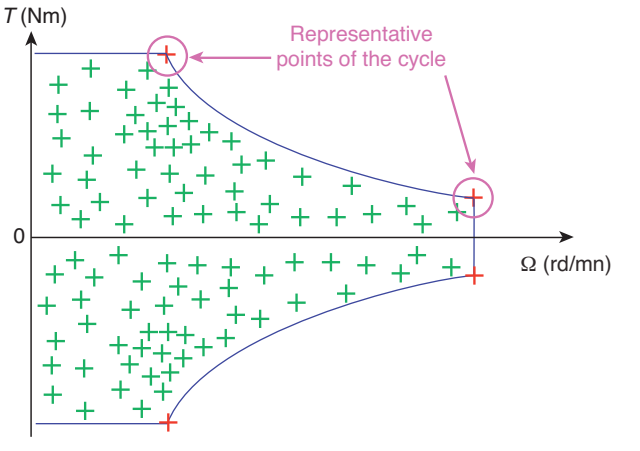

Figure 2

The cycle in the torque *vs* speed plan, and two representative points.

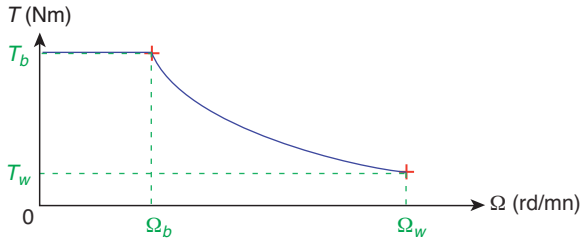

Figure 3

Simple, but significant cycle in the torque vs speed plan. (See Appendix for the numerical values of these requirements).

hybrid vehicle. Nevertheless, such a work needs to take into account the thermal transient states, which is not permitted for the moment by our thermal model. That is why we have decided to perform the optimization for a very simple cycle, composed of two significant points in the torque *vs* speed plan: one point characterized with a high torque and low speed (T_b, Ω_b), and another point with a low torque and high speed named (T_w, Ω_w) *(Fig. 3)*, and these two points must be reached during the same amount of time during the driving cycle. This is a huge simplification of the problem. Moreover, the two points in the plan have to be reached in continuous rate work.

2.1.2 Optimization Parameters

The parameters will be the independent geometrical parameters of the machine (See Appendix for more details concerning these parameters).

2.1.3 Optimization Constraints

There are three kinds of optimization constraints. The first one comes from the motor's design requirements, which consist of being able to reach the points (T_b, Ω_b), and (T_w, Ω_w) required in the torque *vs* speed plan.

Others constraints come from physical criteria, such as no saturation for ferromagnetic parts, or limited temperature rises, or also avoiding demagnetization effects in the magnets. (See Appendix for more details concerning these parameters).

The last constraint comes from the maximum allocated volume for the machine (see Appendix for data about the maximal allocated volume).

2.2 Solving the Problem with Evolutionary Algorithms

Once the optimization problem has been presented, we have to choose a solving method. In such complex and multi-objectives problems, stochastic methods such as evolutionary algorithms are known to be efficient [1]. This is justified by the fact that the objective functions are not convex, so the use of a stochastic algorithm is necessary to avoid local minima. This method consists on choosing at the beginning a random population composed of N_{indiv} individuals, each individual being a parameters array representing a machine topology. Then the objectives' values are calculated for each machine, and the "best" individuals with regard to these objectives will get more chances to reproduce for giving the next generation. Some good individuals can also be cloned, and random mutations can also occur with a low probability. After an important number of generations, the optimal individuals are going to be reached. The illustrated principle, for machine design, is given in Figure 4.

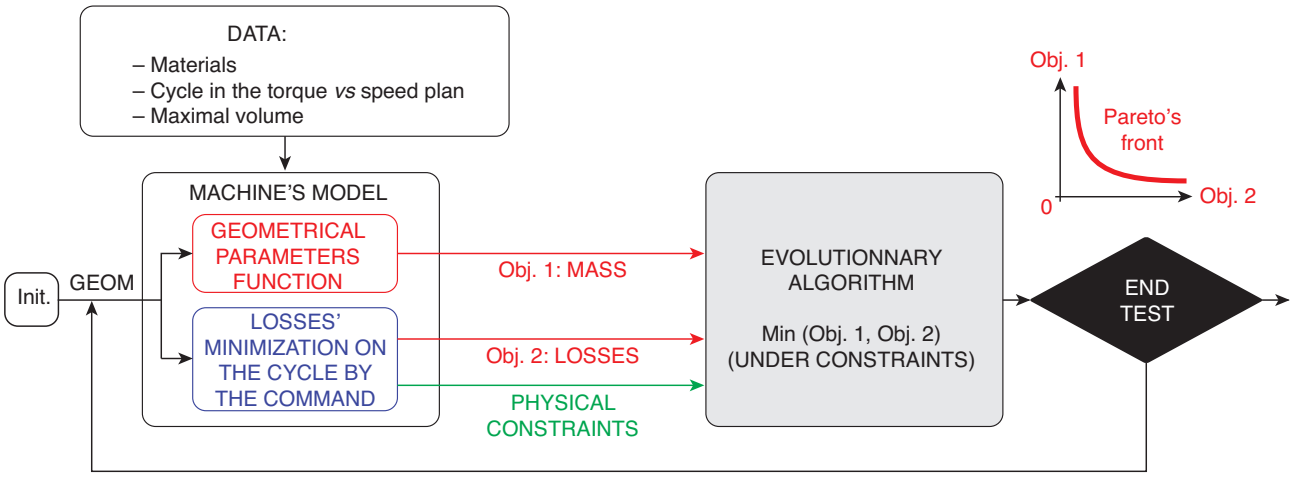

Figure 4

The machine's design strategy.

In fact, it is a bit more complicated *(Fig. 5)*. It is true that the first objective, the mass, can be easily evaluated from the geometrical parameters. Nevertheless, the losses are not only a function of the geometry, but also a function of the way the machine is commanded. It is why, in the model, there is also a local optimization loop which can, given the geometry, determine the best command parameters. This command parameter is in fact the phase displacement Ψ_0 between the electromotive force of the magnets, and the active current *(Fig. 7)*. The other command parameter, which is the modulus nI_0 of the active current in a slot, is related to the angle Ψ_0 given the wished torque (2). The electromagnetic model will be presented in Section 3.1, for the calculation of the magnetic field H, and induction B. The losses model will be introduced in Section 3.4, for the evaluation of the copper losses P_c, and the iron losses P_{iron}. The calculus of thermal resistance is given in Section 3.5, as well as the thermal model, for the determination of the temperatures T in the different parts of the machine. Section 4.1 will present a sensibility study on the nature of the command law.

3 THE MODEL OF THE MACHINE

This paragraph's purpose is to present an analytic model of the axial flux permanent magnet synchronous machine. So it will be possible to carry out an optimal design, by submitting this model to an optimization tool.

3.1 Simplifying Hypothesis

As it was said before, the stator ferromagnetic circuit is laminated, so as to reduce eddy current losses. The windings are put in slots. We only consider the electromagnetic active parts, which are the ferromagnetic parts for the stator and the rotor, the windings and of course, the magnets. These active parts are represented on a mean radius drawing in Figure 6. Let call $\bar{R}$ this mean radius, and $\tau = \pi/p.\bar{R}$ the pole pitch at this mean radius, where p is the number of pole pairs. The relative length of permanent magnets with regard to the pole pitch is named β_{a1}. This winding is composed of three phases, with, for simplification, only one slot per pole. The number of turns per pole is called n, so each slot is filled with $2.n$ wires. The mechanical angular speed of the machine is called Ω.

As it is often the case in electrical engineering, we assume the following points, in order to simplify the problem:

– no saturation effect is taken into account, by limiting the induction in ferromagnetic parts under its saturation value. The magnetic permeability of the ferromagnetic parts is assumed to be infinite;
– end effects are neglected;
– we suppose that continuous rate has been reached, and that the machine is driven with sinus current waves;

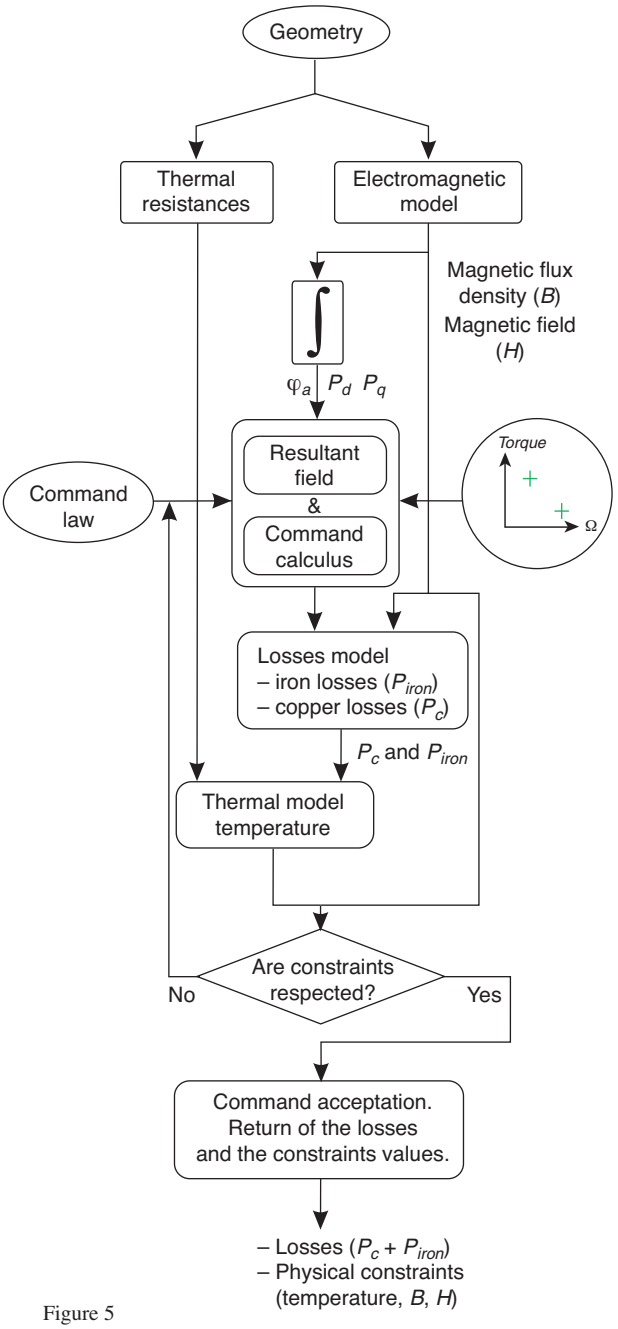

Figure 5

The detailed procedure.

– we consider that the motor is equivalent to a linear actuator which would be obtained by developing the axial flux machine at its mean radius.

Under such hypothesis, the well-known Blondel's theory applied to salient poles synchronous machines permits us to draw the two electric equivalent circuits of Figure 7. There are two different equivalent circuits, since, in the case of salient poles machines, it is necessary to use the Park transformation, consisting on projecting the complex equations of

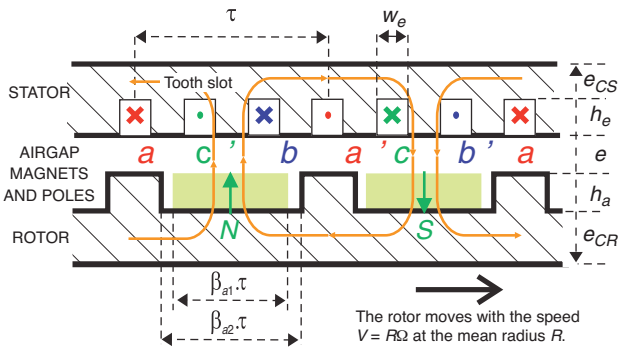

Figure 6

Sectional representation of the machine seen at the mean radius.

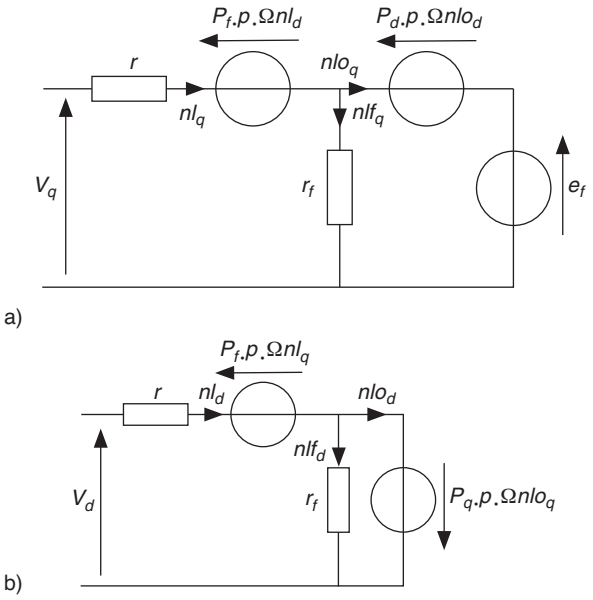

Figure 7

Park equivalent electric circuits of the salient pole synchronous machine. a) The electric equivalent circuit for the *q* axis. b) The electric equivalent circuit for the *d* axis.

the machine along two different axis, which are usually called the *d* axis, and the *q* axis. Instead of directly using the real supply voltage and current, we have chosen to use the voltage per turn, and the currents in a whole coil, in order to be independent of the real supply voltage value. Iron losses are being taken into account, by a resistance r_f.

In Figure 7, the electromotive force caused by the magnets in the stator winding, effective on the *q* axis of the Park base, is called e_f. Saying that $\varphi_{f_{MAX}}$ is the maximal flux under a machine's phase, e_f is equal to:

$$e_f = \frac{\varphi_{f_{MAX}}}{\sqrt{2}} p\Omega \tag{1}$$

The resistance *r* of one phase of the machine is very easy to compute, as the leakage permeance P_f, which is classically evaluated by the magnetic energy stored in the stator slots. Nevertheless, the other parameters, such as $\varphi_{f_{MAX}}$, P_d and P_q, and even r_f, will be more difficult to compute, and we need for that an electromagnetic model.

3.2 Torque Calculation of the Machine

By a simple power balance equation performed in Figure 7, it is possible to compute the torque of the machine:

$$\begin{aligned} T &= 3p\frac{\varphi_{f_{MAX}}}{\sqrt{2}} nIo_q + 3p\left(P_d - P_q\right) nIo_d\, nIo_q \\ T &= 3p\frac{\varphi_{f_{MAX}}}{\sqrt{2}} nIo\cos\left(\Psi_0\right) + \frac{3}{2}p\left(P_d - P_q\right) nIo^2 \sin\left(\Psi_0\right) \end{aligned} \tag{2}$$

Since, thanks to the Park theory of electrical machines, we have:

$$\begin{cases} nIo_d = nIo\cdot\sin\left(\Psi_0\right) \\ nIo_q = nIo\cdot\cos\left(\Psi_0\right) \end{cases} \tag{3}$$

The first term of Equation (2) is called the hybrid torque, while the second term is often called the reluctant torque, only present in salient pole machines. In fact, our electromagnetic model, through the parameters $\varphi_{f_{MAX}}$, P_d and P_q, will permit to calculate this torque.

3.3 The Electromagnetic Model

The goal of the electromagnetic model of the machine is to compute the electromagnetic field in the machine, which is useful both for knowing the iron losses and the non-saturation conditions. Then, an integral of the field may give parameters of the equivalent electric circuits of Figure 7, as the magnets flux, and the inductances. As we said, we are going to use an exact analytical model [3], which is suitable for optimization, because it is faster to compute than numerical methods.

As it is usually the case in electromagnetism, we are going to compute the vector potential, rather than computing directly the induction levels. Thanks to the simplifying hypothesis, the problem can be reduced to the determination of the following vector potential:

$$\vec{A}(x,y) = A(x,y)\vec{u}_z \tag{4}$$

(*x*, *y*, and *z* are the space coordinates defined in *Fig. 8*).

We present here the problem to solve. Figure 8 represents the machine over one pole pitch. For simplicity, the number q_s of stator slots per pole is chosen to be equal to 3, but its value can be changed in the computation procedure.

We compute both the magnetic field produced by the magnets and the one due to the stator currents. In this way, a general expression is derived where, if we only need the no load magnets' flux, the currents' values must be set to zero. For the stator reaction flux, a zero value is given to the

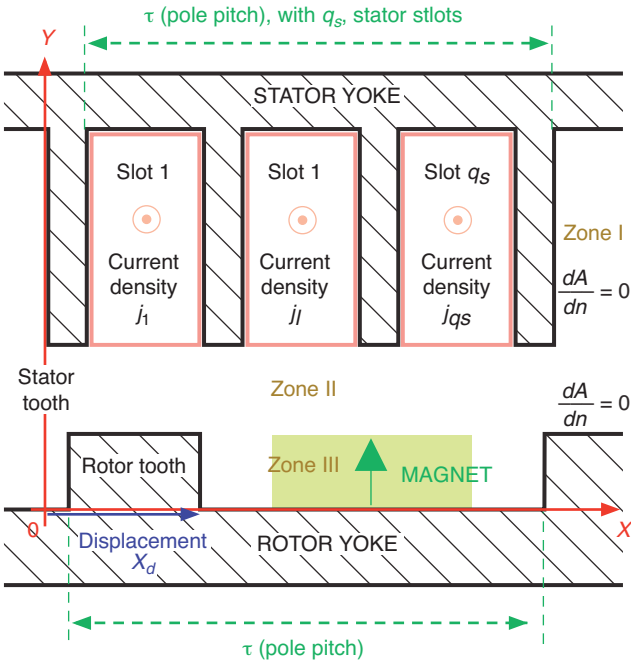

Figure 8

Machine's geometry used in the electromagnetic field computation.

magnets' remanent induction B_r. Taking into account the stator slotting effect is important, since it permits to perform a local and accurate computation of the machine electromagnetic behaviour, even the slots leakage flux lines.

Calling $M(x)$ the magnetization of the magnet which a remanent induction value B_r, the vector potential $A(x, y)$ is given by the following equations:

$$\begin{cases} \Delta A^{(III)} = \mu_0 \dfrac{\partial M}{\partial x} \text{ in zone III} \\ \Delta A^{(II)} = 0 \text{ in zone II} \\ \Delta A^{(I_l)} = \mu_0 j_l \text{ in zone I (slot l)} \end{cases} \quad (5)$$

Moreover, the assumption of ideal ferromagnetic materials imposes a Neumann condition along the iron's edges (both for the stator and rotor):

$$\left.\frac{\partial A}{\partial n}\right|_{iron} = 0 \quad (6)$$

The last Neumann condition is due to the infinite permeability of iron. We solve the problem using developments in the eigen functions of the potential [4, 5]. The expression, in zone I (for a slot number l, l being between 1 and q_s), has been found as: *(Eq. 7)*.

The numbers $a_0^{(l)}$ and $a_m^{(l)}$ will have to be determined by the application of boundary conditions.

The airgap potential has been determined in [5] as:

$$A^{(II)}(x,y) = \sum_{k\geq 1} b_k(y)\cos\left((2k-1)\frac{\pi}{\tau}x\right) + \sum_{k\geq 1} b_k'(y)\sin\left((2k-1)\frac{\pi}{\tau}x\right) \quad (8)$$

Thanks to the Laplace equation, we get:

$$b_k(y) = b_k^{(1)}\cosh\left((2k-1)\frac{\pi}{\tau}y\right) + b_k^{(2)}\sinh\left((2k-1)\frac{\pi}{\tau}y\right) \quad (9)$$

And:

$$b_k'(y) = b_k^{(3)}\cosh\left((2k-1)\frac{\pi}{\tau}y\right) + b_k^{(4)}\sinh\left((2k-1)\frac{\pi}{\tau}y\right) \quad (10)$$

The magnets zone potential (in Zone III) was found in [5] under the following form *(Eq. 11)* where the M_n numbers are dependant on the magnets remanent induction B_r as:

$$M_n = \frac{4}{\pi}\frac{B_r}{\mu_0}\frac{1}{n}\sin\left(n\frac{\beta_{a_1}}{\beta_{a_2}}\frac{\pi}{2}\right)$$

In [5], all the unknown numbers in Equations (7, 9, 10) and (11) were found by applying the boundary conditions of electromagnetism, and forming a Kramer system. Once the vector potential is known, the induction components can be evaluated thanks to the formulae:

$$\begin{cases} B_x = \dfrac{\partial A}{\partial y} \\ B_y = -\dfrac{\partial A}{\partial x} \end{cases} \quad (12)$$

We now propose a verification using finite elements methods. We are going to plot the airgap induction component $B_y(x, y = ha + e)$, x varying between 0 and one pole pitch τ. We performed a calculation using the analytical method, and another with a finite element software. Finally, the method can be tested by comparing the results with a finite element

$$A^{(I,l)}(X_l,Y_l) = a_0^{(l)} + \sum_{m\geq 1} a_m^{(l)}\cosh\left(m\frac{\pi}{w_e}\left(y-\left(h_a+e+h_e\right)\right)\right)\cos\left(m\frac{\pi}{w_e}\left(x-(l-1)\left(w_e+w_d\right)\right)\right) - \frac{1}{2}\mu_0 j_l\left(y-\left(h_a+e+h_e\right)\right)^2 \quad (7)$$

$$A^{(III)}(x,y) = c_0 + \sum_{n\geq 1}\left[c_n\cosh\left(n\frac{\pi}{\beta_{a2}\tau}y\right) - \mu_0\frac{\beta_{a2}\tau}{\pi}\sum_{n\geq 1}\frac{M_n}{n}\cos\left(n\frac{\pi}{\beta_{a2}\tau}\left(x-X_d\right)\right)\right]\cos\left(n\frac{\pi}{\beta_{a2}\tau}\left(x-X_d\right)\right) \quad (11)$$

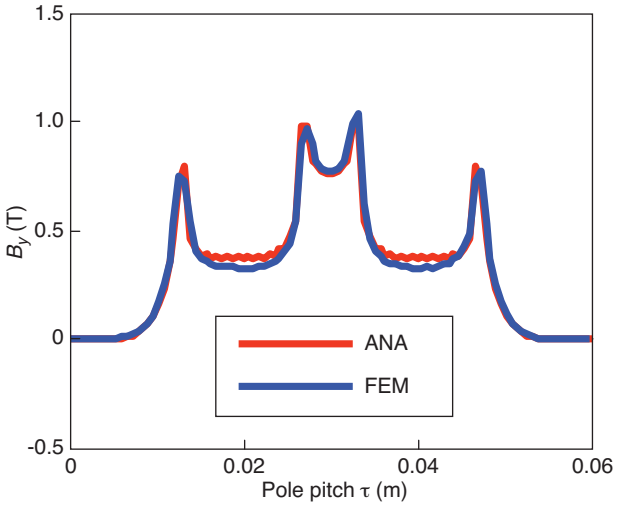

Figure 9

Induction component $B_y(x, y = h_a + e)$ caused by the magnets over one pole pitch.

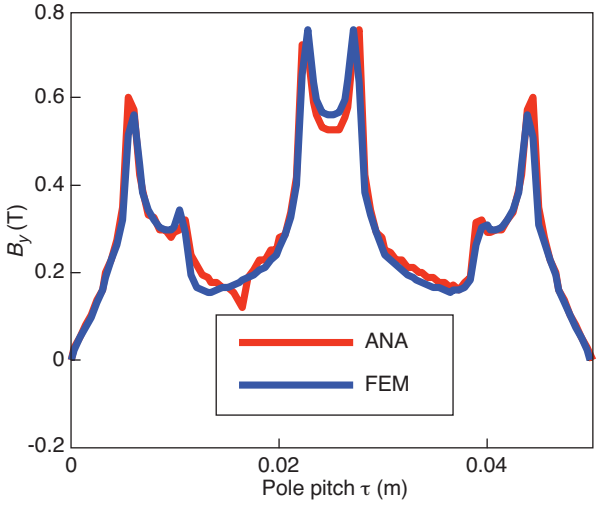

Figure 10

Induction component $B_y(x, y = h_a + e)$ caused by a stator efficient current nI_{0d} = 1000 Atr over one pole pitch, the rotor displacement being equal to $X_d = 0$.

software. For this test, the chosen machine has the following geometry:

- a magnet's thickness of h_a = 3 mm, with a remanent induction B_r = 1.2 T;
- an airgap of e = 0.002 m;
- a pole pitch of τ = 0.05 m;
- the stator and rotor yoke have the same thickness $e_{cr} = e_{cs}$ = 0.01 m;
- the slots' dept is h_e = 0.03 m, and the relative slot opening is 2/3. This signifies that, if we call w_e the slot width and w_d the tooth width, we have the ratio $w_e/(w_e + w_d) = 2/3$. Moreover, the stator presents three teeth and slots over the pole pitch;
- the parameter β_{a2} is equal to 0.8;

A $(0z)$ length H is supposed to be long enough for applying the 2D approximation.

The results are shown in Figure 9 for the magnets excitation, and in Figure 10 for an effective current per slot of nI_0 = 1000 Atr, the rotor displacement being equal to $X_d = 0$. The analytical results are in good accordance, and the computation time is nearly divided by two with the analytical model.

Nevertheless, this analytical model does not permit to take the saturation into account. The same induction component induction component $B_y(x, y = h_a + e)$ obtained with the analytical model and saturated finite elements are plotted in Figure 11. So as to reach saturation in the iron parts, the effective current per slot of nI_0 was put to = 3000 Atr. It can be seen that the induction levels are in the saturated case overestimated by the linear analytical model (by integration we find that there is an error of 20% on the total flux). That is why, as the saturation phenomena is not easy to take into account with an analytical model, and also for optimal command parameters determination, this phenomena will not be taken into consideration. More precisely, the airgap induction under the non saturated hypothesis is deduced, and then the flux in the ferromagnetic parts is calculated using flux conservations law. At the end, the maximal induction in the ferromagnetic parts will be constrained to non-saturation values. This constraint is not a physical constraint like the temperature limit, but that is rather a "model constraint", so as to keep valid the developed model.

Once the induction in the airgap is known, the inductions in the ferromagnetic parts of the machine can be evaluated by flux concentration considerations [6]. We take the example of the stator yoke flux calculation. In the stator teeth, the induction component is assumed to have just a single component, located along the $(0y)$ axis. The calculation method is illustrated in Figure 12. Once, for each coordinate on the tooth Y_t, the induction component $B_t(Y_t)$ is computed using flux concentration consideration: the vector potential components on the left $A_l(Y_t)$ of the tooth, and $A_r(Y_t)$ on the right of the tooth are taken from the previous airgap analytical model. Then, the following formula is applied:

$$B_t\left(Y_t\right) = \frac{A_l\left(Y_t\right) - A_r\left(Y_t\right)}{w_e} \tag{13}$$

In the stator yoke, another method has been used, based on the continuity condition on the potential between the airgap and the ferromagnetic yoke [6]. The calculation principle is explained in Figure 13.

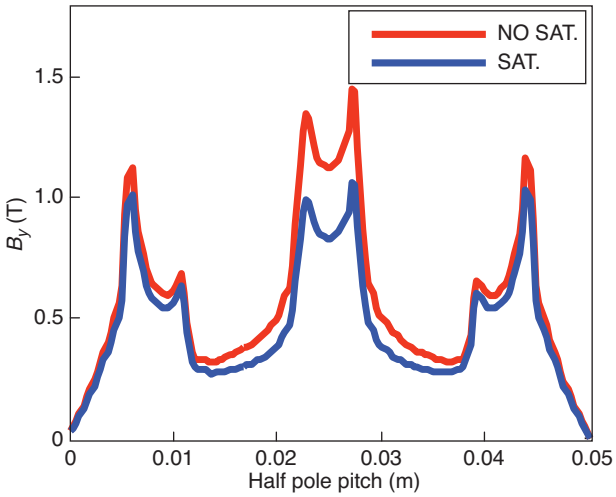

Figure 11

Induction component $B_y(x, y = ha + e)$ caused by a stator efficient current $nI_{0d} = 3000$ Atr over one pole pitch, the rotor displacement being equal to $X_d = 0$, obtained with the linear analytical model on one hand, and saturated finite elements on the other hand.

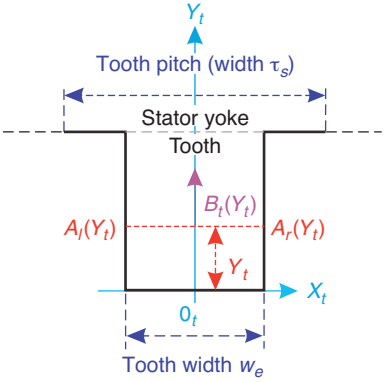

Figure 12

Calculation of the B_y induction in the stator teeth using flux conservation laws.

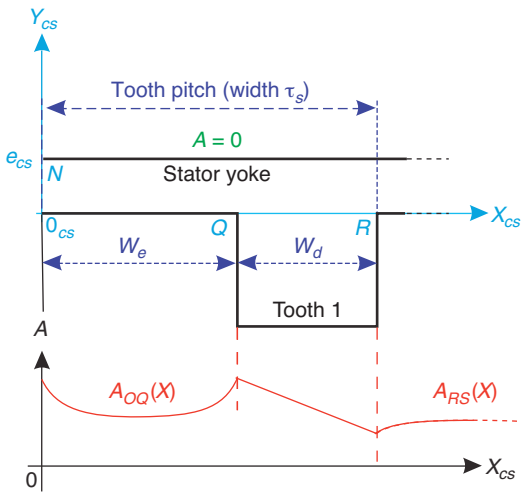

Figure 13

Calculation of the (B_x, B_y) induction components in the stator yoke using flux conservation laws.

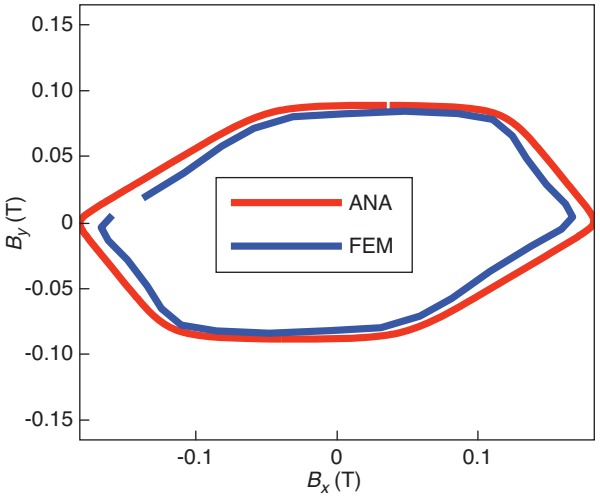

Figure 14

Calculation of the no-load $(B_x(t), B_y(t))$ induction locus in the middle of the stator yoke using the analytical model and finite elements.

On the stator yoke segment [OQ] between the stator yoke and the slot, the evolution of the potential is known, from the calculations in the airgap. On the segment [QR] between the stator yoke and the tooth, the evolution of the potential is assumed to be linear, since the B_y induction component in the tooth was assumed to be uniform. Outside the yoke, the potential is assumed to be zero. Then, the potential is known at every point of the boundary of the stator yoke. Given the Laplace equation of the vector potential, the eigen function method permits to find the vector potential in the yoke by solving the Dirichlet problem, and then the two components (B_x, B_y) of the induction at each point of the yoke. This calculation has been repeated for each elementary position of the rotor over one pole pitch, and then the time dependency can be found. As an example, the no-load flux locus $(B_x(t), B_y(t))$ in the middle of the rotor yoke has been computed, both with the analytical model and finite elements. The results are shown in Figure 14, and the agreement between the two methods is satisfying. This method has the advantage of giving the two components $(B_x(t), B_y(t))$ of induction in the stator yoke.

A similar method is used in the rotor yoke and saliency. This is useful for writing a correct no-saturation condition of the rotor ferromagnetic parts. Nevertheless, the time variation of the rotor induction is neglected, and iron losses are

computed only in the stator. It can be seen that the induction waveforms are not at all sinusoidal (the induction locus presented in Figure 14 is not elliptic). So an iron losses model giving the iron losses even under non-sinusoidal waveform is required.

3.4 Copper and Iron Losses

We are going to compute the copper losses and the iron losses.

Copper losses are given by the formula:

$$P_C = 3r\left(nI_d^2 + nI_q^2\right) \tag{14}$$

The resistance r includes the one of the winding overhangs. We recall that the currents have been evaluated thanks to the optimization of the command, once the geometry is given.

The deduction of iron losses per unit volume at the point (x, y) will be made by using Bertotti's classical formulation [8, 9], taking into account the non-sinusoidal properties of the waveforms, as well as the minor loops:

$$\begin{aligned} p_{iron}(x,y) &= k_{H_1}.\Delta B_{pp}.f + k_{H_2}.\Delta B_{pp}{}^2.f \\ &+ 2.\sum_{\text{minor loops}} k_{H_1}.\Delta B_{pp_{ML}}.f + k_{H_2}.\Delta B_{pp_{ML}}{}^2.f \\ &+ \alpha_p.\left(\frac{dB}{dt}\right)_{eff}^2 + k_{exc}.\left(\frac{dB}{dt}\right)_{eff}^{3/2} \end{aligned} \tag{15}$$

where k_{h1} and k_{h2}, α_p and k_{exc} are constant representative of respectively hysteresis losses, classical losses and hysteresis losses in the ferromagnetic material.

To take into account the two dimensional property of the induction, as it is often done in electrical engineering, we independently compute the losses in the two directions with Equation (15), and then sum up the losses along the two axis. This problem does not arise in the teeth zone, since it was assumed in the model that the induction was only along the (Oy) axis. Nevertheless, it is useful in the stator yoke losses computation.

The total iron losses P_{iron} in the stator are then evaluated by integration on all the stator volume. This value is useful for the computation of the resistance r_f in Figure 7.

The constant used in this model about the materials are given in the appendix.

3.5 Thermal Model

We are going to build a thermal model with the assumption of continuous rate. So it will be possible to calculate temperature rises in the different parts of the machine. Then, the copper wires temperature is going to be constrained to an upper value during the optimization process, so as to avoid the destruction of the wires insulator material.

The simplifying assumptions of the thermal model are the following:

- continuous rating is assumed to be reached;
- since the machine is water-cooled, we suppose that the water circulation is the only way to cool the machine. All other convective heat transfer, such as direct air cooling of the winding overhangs, are assumed to be negligible. The convective thermal resistance between the stator yoke and water is assumed to be zero (perfect thermal contact);
- heat radiation transfer is also neglected;
- the thermal model, just as the electromagnetic one, is assumed to be bi-dimensional, and developed at the machine's mean radius;
- the heat transfer in the ferromagnetic stator yoke known for having a good thermal conductivity λ_{iron} = 72 W/(K.m), is assumed to be uni-dimensional along the (0y) axis. This assumption will be verified using thermal finite elements;
- the slot zone is assumed to be homogeneous. The thermal conductivity of this zone composed of the wires, the insulator around them, and air between the wires is evaluated experimentally. A numerical value of λ_{slot} = 0.04 W/(K.m) has been found;
- it is also assumed that copper losses are more difficult to evacuate than the iron losses, so that the hottest point of the stator yoke is located in the middle of the slot *(Fig. 15)*;
- the losses are assumed to be uniform in the stator ferromagnetic tooth and yoke, taken equal to their mean value given by the iron losses model.

Assuming an unidirectional heat transfer, the thermal resistances R_{THy} and R_{THi2} are computed using the classical formulae of conductive heat transfer, calling λ_{iso} = 0.143 W/(K.m):

$$R_{THy} = \frac{1}{\lambda_{iron}} \frac{e_{cs}}{\frac{1}{2}\left(w_e + w_d\right)\cdot \Delta R} \tag{16}$$

And:

$$R_{THi2} = \frac{1}{\lambda_{iso}} \frac{e_{iso}}{\left(\frac{w_e}{2} - e_{iso}\right)\cdot \Delta R} \tag{17}$$

The other thermal resistances are more difficult to compute, since they involve bi-directional heat transfer. The calculation is performed using the eigen function development of the Poisson equation describing the conduction heat transfer. Calling p_C and p_T the losses volume densities in the slot and in the tooth, these equations are:

$$\begin{cases} \Delta T = -\dfrac{p_C}{\lambda_{slot}} & \text{in the slot} \\ \Delta T = 0 & \text{in the insulator} \\ \Delta T = -\dfrac{p_T}{\lambda_{iron}} & \text{in the tooth} \end{cases} \tag{18}$$

After solving this differential system, the thermal resistances can be evaluated.

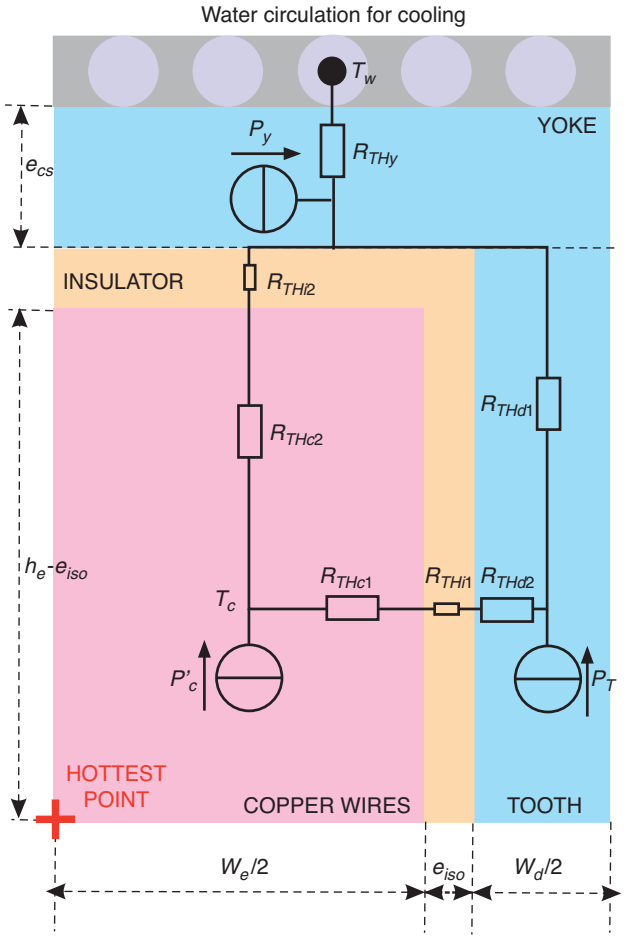

Figure 15

Thermal model of a half slot and a half tooth.

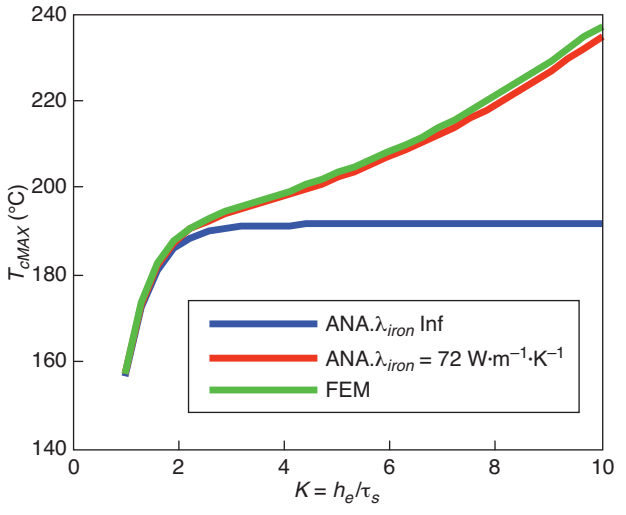

Figure 16

Evaluation of the maximal temperature of the copper, using analytical methods, and thermal 2D finite elements.

Then, using the lumped thermal model of Figure 15 (p_C' is the copper losses for a half slot, p_T is the losses for a half tooth and p_Y represents the yoke losses in a half tooth pitch), the maximal temperature of the copper can be calculated.

To verify this thermal model, a 2D thermal simulation has been carried out. We take the following geometry:

- the airgap dimensions are the same as the ones used for the electromagnetic simulations;
- the stator yoke thickness is $e_{cs} = 0.01$ m;
- the losses densities in the yoke, the slot, and the tooth are taken equal to, respectively: $p_Y = 10^3$ W/m^3, $p_C = 10^5$ W/m^3, and $p_T = 10^4$ W/m^3;
- an insulation thickness $e_{iso} = 2{\cdot}10^{-4}$ m;
- the slot dept h_e varies from w_e to $10w_e$. This will permit to understand what happens if the temperature drops along the ferromagnetic parts is not taken into account, that is to say if λ_{iron} is taken as infinite.

For each geometry, the maximal temperature of the copper is calculated. The result is given in Figure 16.

Although the 1D heat transfer assumption in the stator yoke, the results obtained with thermal finite elements and the analytical model are very similar. Moreover, it becomes clear that, even if the iron thermal conductivity is high, taking it as infinite may lead to significant error, particularly if the slot dept h_e becomes high. This is very important in an optimization purpose, since such an error may lead the optimization algorithm to propose very narrow slot geometries, although this leads in reality to excessive heating of the wires.

4 RESULTS PRESENTATION AND ANALYSIS

In this paragraph, we are going to present, and discuss some optimization results.

In a first part, we are going to study the influence of the chosen command law on the machine design. Then, the nature of the magnets is going to be studied. No inverter restriction is being taken into account.

4.1 Influence of the Machine's Command Law

As we said in the previous paragraph, the local optimization procedure of the machine can compute the optimal command law for the two working points given the geometrical parameters. This optimal command law finds the command parameters satisfying all the physical restrictions and the torque requirements, while giving the minimum sum of iron and copper losses. We wonder what would happen if, as it is often done for simplicity, we choose to minimize only the copper losses, and not the sum of iron losses and copper losses. We call Ψ_0 the phase displacement between the active current nI_0 and the magnets electromotive force e_f.

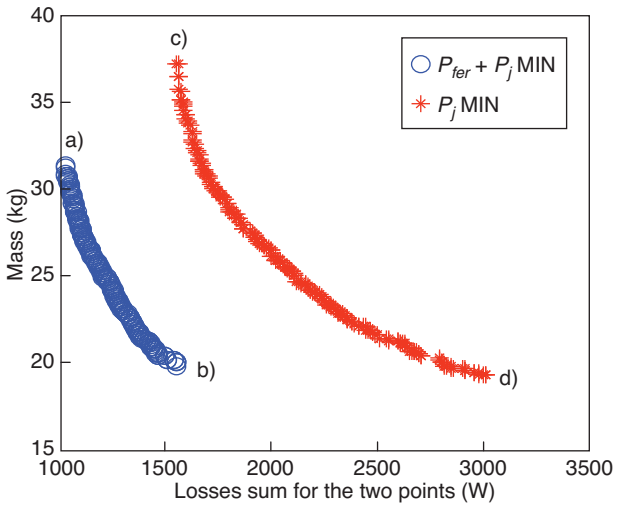

Figure 17

Comparison of two different command strategies.

This minimization problem of the copper losses is classical: in reference [7], it is proven that, for a salient pole machine, there is an optimal value $\Psi_{0opt} < 0$, due to the reluctant torque term.

The optimization results are shown in Figure 17 for the Pareto curves and Figure 18 for the machines geometries.

The Pareto's curve is better by trying to minimize the sum of iron and copper losses. The best reachable efficiency in a volume of 9.4 L is $\eta_{opt} = 0.97$ if the sum of the losses is locally minimized, whereas it becomes $\eta_{opt} = 0.93$ if only the copper losses are locally minimized. The best torque per unit mass does not change a lot between the two command strategies, being approximately equal to 5 Nm/kg. The number of pole pairs (proposed by the optimizer), is, roughly speaking, between 10 and 20.

We are going to explain the difference on the losses: taking into account iron losses leads the optimization tool to design machines with flux weakening capabilities, even if no voltage constraint is applied, since the injection of a significative current $nI_{0d} < 0$ at the high speed-low torque point can drastically reduce the resulting flux in the machine, and then the iron losses. This reduction of the iron losses is especially suitable for the high speed-low-torque point (T_w, Ω_w). This field weakening effect is illustrated in Figure 19: the phase displacement Ψ_0 used for the high speed-low torque point is given, and we can see that for the machine with flux weakening capabilities, the value is very closed to –90°. It is possible to verify in Figure 20 that at the high speed-low-torque point (T_w, Ω_w), the iron losses are much more important for the machine with no field weakening capabilities (they are multiplied by a factor going from 4 for the biggest machines, to seven for the smallest ones).

It is also possible to notice that the necessity of reducing the iron losses at the high speed-low-torque point (T_w, Ω_w) also have an impact on the geometry of the machines. For example, comparing the machines (a) and (c) in Figure 18 (these are the biggest machines, for which the efficiency criteria is the most important), the reduction of the iron losses if flux weakening is not allowed (see machine (c)) leads to a significant augmentation of the stator yoke volume. Then the

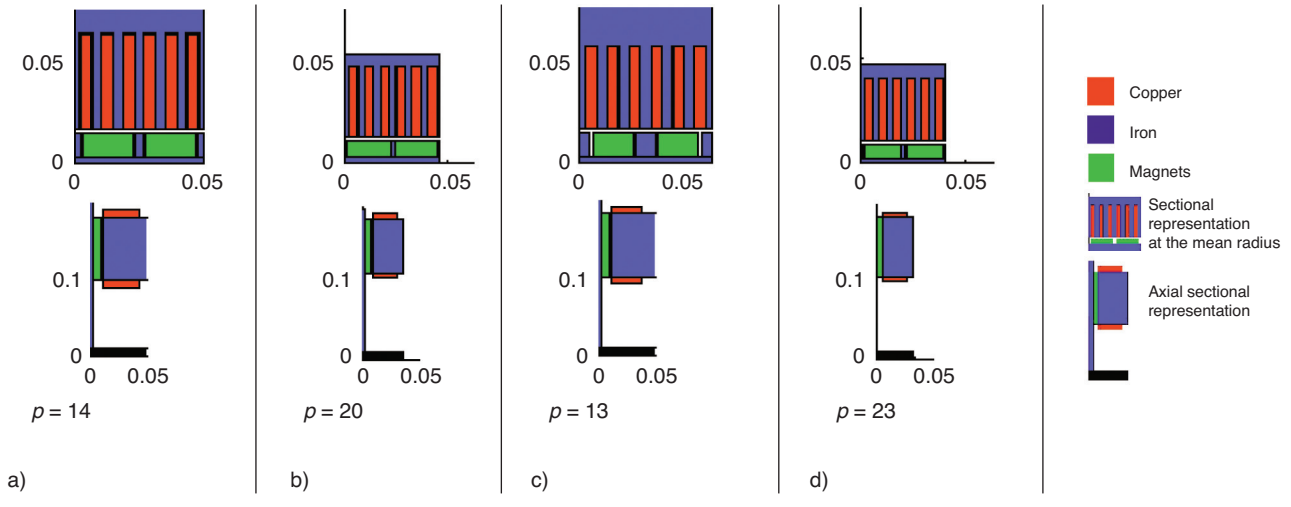

Figure 18

Geometry of the extreme of the Pareto curves.

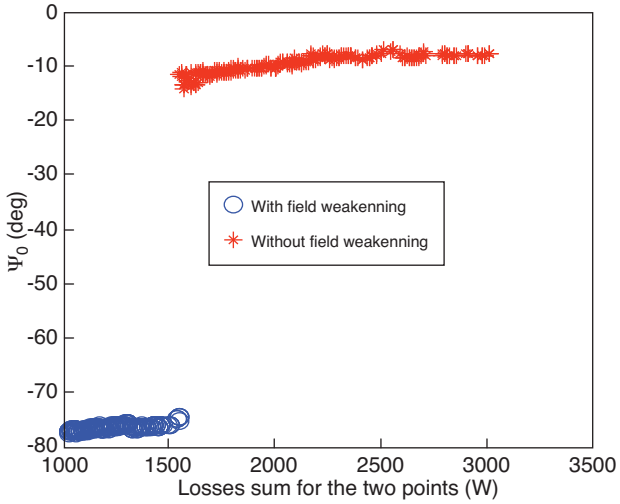

Figure 19

Angles Ψ_0 for the point high speed/low torque point (T_w, Ω_w).

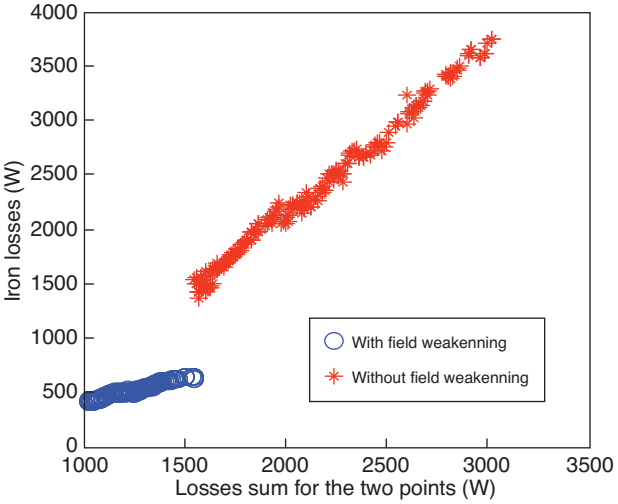

Figure 20

Iron losses for the point high speed/low torque point (T_w, Ω_w).

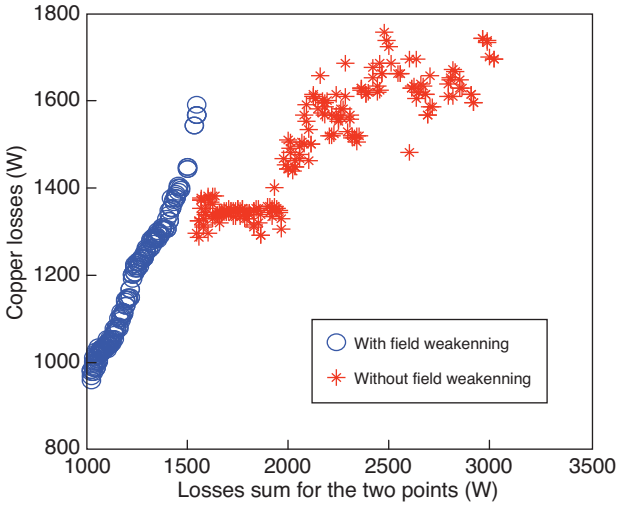

Figure 21

Copper losses for the low speed/high torque point (T_b, Ω_b).

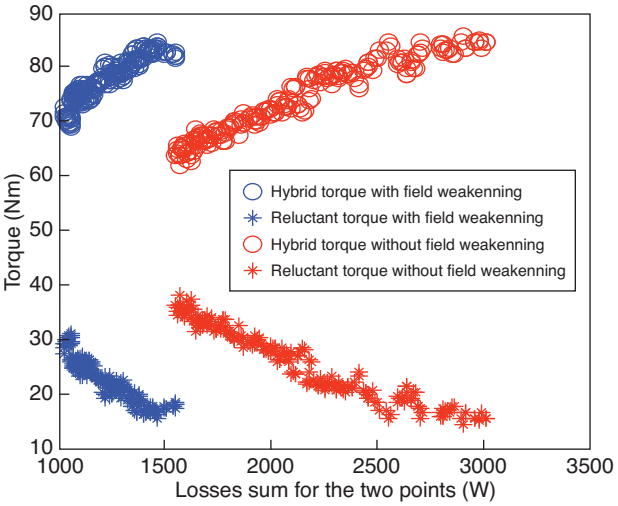

Figure 22

Hybrid and reluctant torque values for the low speed/high torque point (T_b, Ω_b), the total torque to reach being T_b = 100 Nm.

available space for the copper is reduced, leading to an increase of the current density in the slots, and so to a copper losses increase for the low-speed-high torque point (T_b, Ω_b). This phenomenon is amplified by the fact that the magnets volume is less important for the machine (c), always for the limitation of the iron losses. This implies that, for reaching the low-speed-high torque point (T_b, Ω_b), the hybrid torque proportion is reduced, whereas the relative part of the reluctant torque is increased. In this purpose, the saliency effect is increased in the machines with no flux weakening, by using a large rotor tooth. These explanations can be verified in Figure 21 and Figure 22, on which the copper losses and the different torques for the low-speed-high torque point (T_b, Ω_b) are plotted. Nevertheless, this explanation does not hold for the smallest machines, since, even if the magnets can cause higher iron losses, the efficiency criteria is not a problem for such machines: even if flux weakening is prohibited, the smallest machines (machine (d) in *Fig. 18*) tend to have an important magnet volume, because the hybrid torque can help reach the low-speed-high torque point with less current than the reluctant torque, then allowing a decrease of the machine's copper mass.

We finish by saying that, even if no voltage limitation has been introduced in this optimization procedure, it can be seen

in Figure 23 that the flux weakening command strategy requires a much smaller inverter apparent power.

4.2 Influence of the Magnets' Type

For the previous study, the magnets used are ferrite magnets, with a remanent induction at 25°C B_{r0} = 0.3 T. We shall now study what happens on the Pareto front if the remanent induction of the magnets is changed. For example, we can try to replace the ferrite magnets by NdFeB magnets. A lot of variants of NdFeB magnets exist, their remanent induction B_{r0} at 25°C going from 0.7 T to 1.2 T. That is why given the same volume and torque requirements, the optimizations will be carried out with a remanent induction B_{r0} = 0.7 T, and another with B_{r0} = 1.2 T. The obtained Pareto curves are presented in Figure 24, and the extreme machines in Figure 25. The immediate conclusion that can be drawn out is that an increase of the remanent induction from B_{r0} = 0.3 T to B_{r0} = 0.7 T seems to be an efficient way to improve both the torque per unit mass and the efficiency.

This result is explained by the fact that a high remanent induction level for the magnets permits to reach the low speed-high torque point (T_b, Ω_b) with lower currents, so the copper losses are significantly reduced *(Fig. 26)*. Nevertheless,

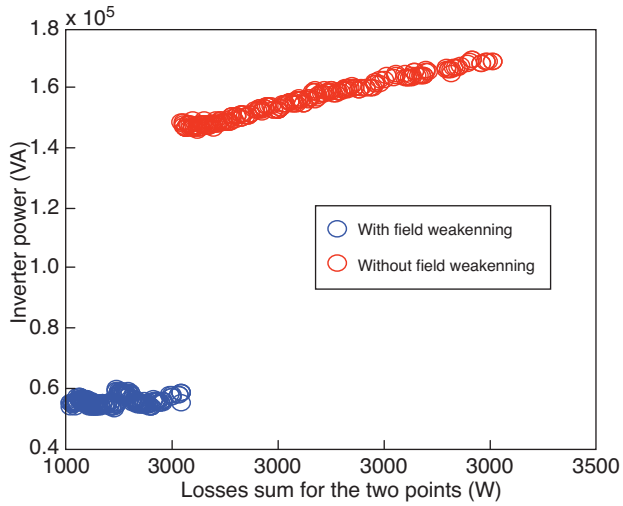

Figure 23

Necessary apparent power.

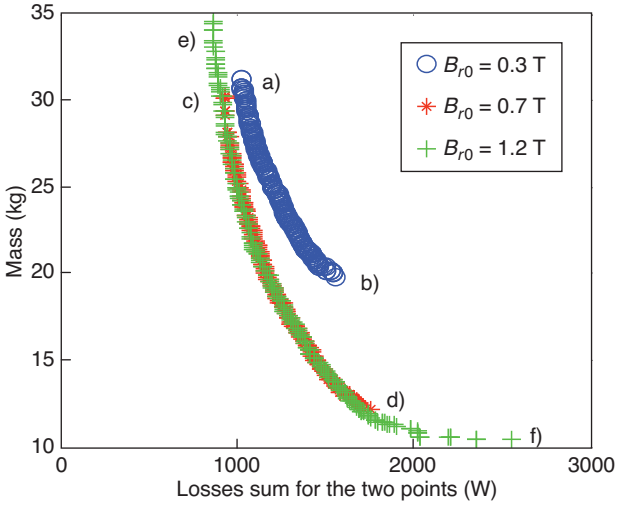

Figure 24

Pareto's curves for different remanent inductions of the magnets.

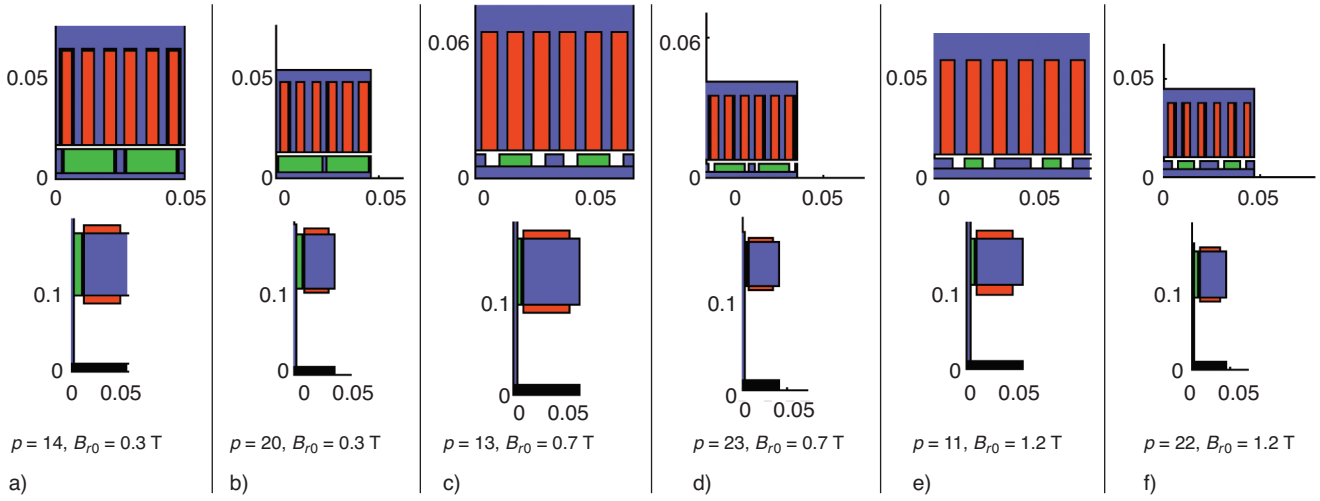

Figure 25

Geometry of the extreme of the Pareto curves.

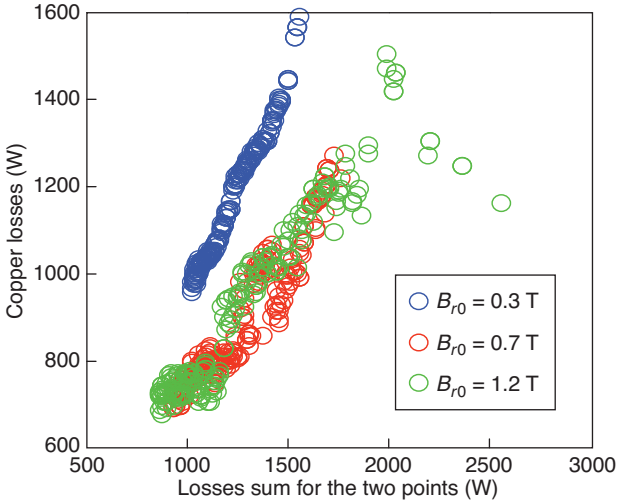

Figure 26

Copper losses for the point (T_b, Ω_b) for the three magnets.

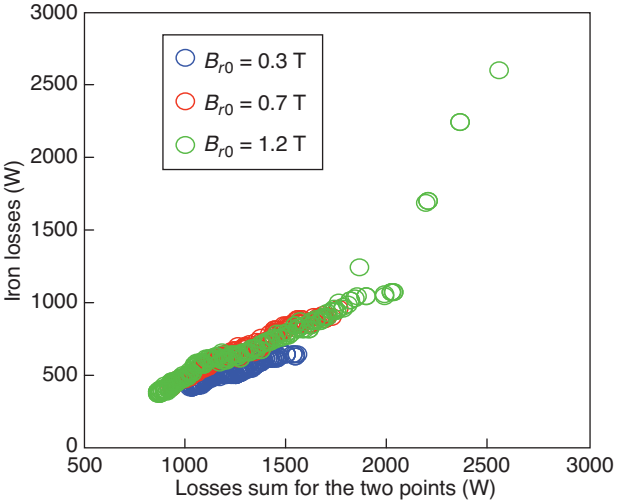

Figure 27

Iron losses for the point (T_b, Ω_w) for the three magnets.

higher magnets flux also mean higher iron losses when reaching the high speed-low-torque point (T_w, Ω_w) *(Fig. 27)*, and a compromise has to be found between the magnets flux permitting to reduce the copper losses for the low speed-high torque point (T_b, Ω_b), and the generation of higher iron losses at the high speed-low-torque point (T_w, Ω_w).

On the contrary, it can be seen that taking a remanent induction B_{r0} = 1.2 T instead of B_{r0} = 0.7 T does not improve the machine capabilities. This is due to the teeth saturation constraint, and the necessity of limiting the iron losses for the high speed. So as to respect these requirements without reducing too much the slot size (which would be then a problem for the injecting a significant current in the slots), the optimizer has chosen to put very small magnets (*Fig. 25*, machine (e)). This strategy has the advantage of permitting to put very large rotor teeth, which is necessary for the flux weakening (the L_d inductance is much higher). Moreover, important magnets with a high remanent induction would increase too much the iron losses. That is why one can notice in Figure 26 the following rather surprising fact: although the magnet has a higher remanent induction of B_{r0} = 1.2 T, the copper losses for the low speed-high torque point (T_b, Ω_b) are not lower (they even tend to be superior). And the iron losses *(Fig. 27)* are nearly the same for the two NdFeB machines.

Nevertheless, the highest remanent induction can be interesting if the only important parameter is the torque per unit mass. For the extreme machine (f), one can see that the following strategy has been chosen, so as to reach the best torque per unit mass: the maximum amount of magnet before reaching the saturation constraint has been used. The iron losses are not a problem, because for this extreme machine, the torque per unit mass is the only important parameter, and because iron losses have a reduced influence on the thermal model. That is why the iron losses for the high speed-low-torque point (T_w, Ω_w) are very high. So, for respecting the stator teeth saturation constraint, as the stator teeth are quite large, the slot width is reduced. Nevertheless, that is not an important problem, since thanks to the high magnets flux, the currents keep limited values. Moreover, these configurations with very thin slots and large teeth are interesting from a thermal point of view, since the teeth iron behaves as a cold source to cool the slots. Then a high copper losses density is possible before reaching the copper thermal limit.

CONCLUSION

This article presents an optimal design tool for axial flux permanent magnets machines, using an exact analytical model, for the magnetic field computation. Others physical models, such as the thermal one, permit to clearly understand the design problems of such machines. Moreover, the influence of the command law has been shown, and the problem of inverter design, important for an embedded application. Further work can consist on improving the model of iron losses, taking into account more precisely the bi-dimensional aspect of the magnetic field in a better way than previously. Another possible way is to consider a whole working cycle of the hybrid vehicle. So as to carry out this analysis, it would be necessary to build thermal transient model. To finish, another interesting thing would be to consider all the parts of the hybrid vehicle, including the thermal motor, and

not only the electric machine. So it would be possible to perform a real system optimization, with such criteria as the vehicle's mass, and fuel consumption.

REFERENCES

1 Tenconi A., Profumo F. (1996) Axial flux machines drives: a new viable solution for electric cars, *Proc. IEEE Taipei* **44**, 39-45.

2 Deb K. (2002) *Multi-Objective Optimization using Evolutionary Algorithms*, John Wiley & Sons, LTD, ISBN 0-471-87339.

3 Régnier J. (2003) Résolution de problèmes multicritères par des méthodes évolutionnaires pour l'optimisation directe de systèmes hétérogènes en Génie Électrique, *Thèse*, Institut national polytechnique de Toulouse.

4 Sargos F.M., Rezzoug A. (1991) Calcul analytique du champ engendré par les aimants dans l'entrefer d'une machine à pôles saillants, *J. Phys. III* **1**, 103-110.

5 Goldbar P., Stone M. (2009) *Mathematics for Physic: a guided tour for graduate students*, Cambridge University Press.

6 de la Barrière O., Ben Ahmed H., Gabsi M. (2009) Computation of the magnetic field in the stator in the airgap of an axial flux permanent magnet machine taking into account the stator and rotor saliency, *IEEE T. Magn.* (to be published).

7 de la Barrière O., Ben Ahmed H., Gabsi M. (2009) 2D analytical ferromagnetic parts' model of an insert PM machine, *IEEE T. Magn.* (to be published).

8 Amara Y. (2001) Contribution à la commande et à la conception des machines synchrones à double excitation, *Thèse*, Université Paris Sud 11.

9 Bertotti G. (1984) A general statistical approach to the problem of eddy current losses, *J. Magn. Magn. Mater.* **41**, 253-260.

10 Bertotti G. (1988) General properties of power losses in soft magnetic materials, *IEEE T. Magn.* **24**, 621-630.

11 Belicova E., Hrabovcova V. (2007) Analysis of an Axial Flux Permanent Magnet Machine (AFPM) based on coupling of two separated Simulation Models (Electrical and Thermal ones), *J. Electrical Eng.* **58**, 3-9.

Final manuscript received in August 2009
Published online in November 2009

APPENDIX

1. The machine's requirements and restrictions.

Torque and Speed requirements	$T_b = 100$ N.m $\Omega_b = 2700$ rd/mn $T_w = T_b/6$ $\Omega_w = 6.\Omega_b$
Maximal allocated volume	$R_{extMAX} = 20$ cm $L_{aMAX} = 7.5$ cm
Physical constraints	$B_{iron} < 1.5$ T $H_{magnet} > -Hk$ (demagnetizatisation field) $T_{copper} < 180°C$ $w_e > w_{eMIN} = 2$ mm (minimal width for the stator slot)

2. The detail of independent geometrical parameters.
(See *Fig. 6*, which is the representation at the mean radius of the machine, for a representation of some of the parameters).

e_{cs}	Thickness of the stator yoke (m)
e_{cr}	Thickness of the rotor yoke (m)
h_a	Thickness of the rotor yoke (m)
h_e	Thickness of the tooth zone (m)
R_2	External radius of the rotor (m)
R_1	Internal radius of the rotor (m)
β_{a2}	Relative length between two rotor poles
β_{a1}	Relative length of the magnets
w_e	Thickness of one slot (m)
p	Number of poles pairs

3. Data about the materials.

Iron losses data: FeSi 3% iron lamination, with 0.35 mm for the lamination thickness	$k_{h1} = 12$ A/m $k_{h2} = 90$ Am/Vs $\alpha_p = 2700$ rd/mn $k_{exc} = 0$ (for the moment) density: 7700 kg/m^3
Copper data	Resistivity: $\rho = 1.72e\text{-}8$ Ωm at 25°C (0.4% increase per degree) density: 8800 kg/m^3